Journal of Electroceramics, 13, 677–682, 2004
© 2004 Kluwer Academic Publishers. Manufactured in The Netherlands.

Interaction between Water and Ceria-Zirconia-Yttria Solid Solutions

N. SAKAI,* K. YAMAJI, Y.P. XIONG, H. KISHIMOTO, T. HORITA & H. YOKOKAWA
National Institute of Advanced Industrial Science and Technology (AIST), AIST Central 5, Higashi 1-1-1, Tsukuba 305-8565, Japan

Submitted February 13, 2003; Revised February 5, 2004; Accepted March 19, 2004

Abstract. We have investigated the water solubility, oxygen isotope diffusivity, and oxygen surface exchange coefficient in a humid atmosphere of the system $\{(CeO_2)_x(ZrO_2)_{1-x}\}_{0.8}(YO_{1.5})_{0.2}$ ($x = 0$–1) by using isotope exchange and secondary ion mass spectrometry (SIMS). The deuterium ion ($^2D^-$) was detected from the $\{(CeO_2)_x(ZrO_2)_{1-x}\}_{0.8}(YO_{1.5})_{0.2}$ polycrystals which were annealed in D_2O containing atmosphere. The solubility of deuterium in the polycrystals increased with the cerium content (x). The oxygen exchange rate constant (α) in air at $T = 973$ K shows a maximum at $x = 0.2$–0.3, which can be correlated to the compositional dependence of electronic conductivity of $\{(CeO_2)_x(ZrO_2)_{1-x}\}_{0.8}(YO_{1.5})_{0.2}$. The effect of water on the surface exchange rate constant was more significantly observed for the samples with higher content of cerium $x > 0.6$.

Keywords: ceria, zirconia, diffusion, water vapor, surface reaction

1. Introduction

In solid oxide fuel cells (SOFC), ceria-zirconia-yttria solid solution (CeO_2-ZrO_2-$YO_{1.5}$) with cubic fluorite structure was initially investigated as the reaction compounds found at the interface of yttria stabilized zirconia (YSZ) electrolyte and yttria doped ceria (YDC) as anode or cathode interlayer [1]. The combination of YSZ and rare earth doped ceria is often adopted to cope with both chemical stability of YSZ and high catalytic activity of ceria. Doped ceria layer is also introduced between YSZ electrolytes and cathode materials, such as lanthanum cobalt oxides to prevent the undesirable reaction forming $La_2Zr_2O_7$. However, when YSZ and doped ceria is co-fired at high temperatures, the interdiffusion of cerium and zirconium components is often observed at the interface, which results in the formation of CeO_2-ZrO_2-$RO_{1.5}$ (R: trivalent rare earths) solid solutions [2]. The low electrical conductivity of the CeO_2-ZrO_2-$RO_{1.5}$ solid solutions may have a bad influence on the cell performance [3].

On the other hand, ceria-zirconia solid solutions have been investigated from viewpoints of interesting catalytic activity and mixed conductivity. Bozo et al., reported the CeO_2-ZrO_2 solid solution as a promising support material for catalysts of methane oxidation [4]. Since methane is one of the most popular fuels for SOFC, the CeO_2-ZrO_2 solid solution can be also used as anode additives for SOFC. Moreover, the CeO_2-ZrO_2-$YO_{1.5}$ solid solution is investigated as a promising material for oxygen permeable membranes, which can be applied to electro-catalytic reactors or oxygen gas separators. The temperature and oxygen partial pressure dependence of total and ionic conductivity of $\{(CeO_2)_{1-x}(ZrO_2)_x\}_{0.9}(Y_2O_3)_{0.1}$ have been reported by several researchers [5–7]. These electrochemical devices are operated at very high temperatures, and sometimes under a very large gradient of oxygen partial pressures.

We have investigated the oxygen and proton transport properties of those solid solutions because such properties are closely related to the ionic conductivity or catalytic activity in redox reactions. The combination of isotope exchange and secondary ion mass spectrometry (SIMS) was a powerful technique to determine the solubility, diffusivity and surface exchange rate constants of oxygen and hydrogen in solids. We have already reported the oxygen isotope diffusivity and surface exchange rate constant for $\{(CeO_2)_{1-x}(ZrO_2)_x\}_{0.9}(Y_2O_3)_{0.1}$ solid solutions at 973 K in dry air and in CO_2-H_2 mixtures [8]. The

*To whom all correspondence should be addressed. E-mail: n-sakai@aist.go.jp

electronic and hole conductivities are also important factors to examine the electrochemical reaction mechanism, and we have already measured those conductivities by using a Hebb-Wagner blocking method [9]. Furthermore, we have found that rare earth doped ceria polycrystals exhibit a significant absorption of water vapor at high temperatures [10], and the oxygen exchange rate constant on YSZ or gadolinium doped ceria (GDC) surfaces drastically increased with the addition of a slight amount of water vapor in gaseous atmosphere [11–13]. Hence it would be interesting to investigate how the effect of water will appear in ceria-zirconia solid solutions.

In this paper, we report the water solubility, the oxygen isotope diffusivity and surface exchange rate of $\{(CeO_2)_x(ZrO_2)_{1-x}\}_{0.8}(YO_{1.5})_{0.2}$ polycrystals as a function of cerium content x using the annealing in D_2O or $H_2^{18}O$ containing atmosphere and subsequent SIMS analyses. The correlations with other transport properties such as ionic and electronic conductivities are also discussed.

2. Experimental

The sample composition adopted in the present study was $\{(CeO_2)_x(ZrO_2)_{1-x}\}_{0.8}(YO_{1.5})_{0.2}$ ($x = 0, 0.1, 0.2, \ldots 1.0$). For preparation of the dense polycrystals, an appropriate amount of CeO_2, Y_2O_3 (Wako Pure Chemicals Co. Japan), and ZrO_2 (TOSOH TZ-0, Japan) powders were mixed by TZP ball milling in ethanol as solvent for 7 days. After drying powder mixtures on a hot plate, the powders were pressed into pellets (22 mm in diameter and 3 mm thick) by one-axial pressing ($p = 150$ MPa) and cold iso-static pressing ($p = 300$ MPa). The pellets were then sintered at $T = 1923$ K for 10–20 hours in air. The relative densities of the sintered pellets were above 96%. The surface of each pellet was polished using diamond paste.

For determination of water solubility, the samples were annealed in gas mixture of 2% O_2 + 2% D_2O (99.9% enriched ^{2}D, ISOTEC Co. Ltd.) + 96% N_2 at 973 or 1173 K for 60 h. The total flow rate of the gas mixture was kept at 100 ml/min until the samples were rapidly cooled to room temperature. The depth profiles of the intensities of $^1H^-$, $^2D^-$, $^{16}O^-$ and $^{89}Y^{16}O^-$ ions in the samples were collected by SIMS (ims5f, CAMECA Instruments Co. Primary Ion: Cs^+ 10 kV).

For determination of oxygen isotope diffusivity and surface exchange rate in a humid atmosphere, the sample was placed in a small exchange cell with a thermocouple (R-type, Pt-Pt(Rh)) connected to a closed system. To avoid any catalytic effect of platinum, ceramic wool was placed around the sample. For pre-annealing, the treatment cell was connected to one section of closed system where normal O_2 and D_2O was introduced, and kept at 973 K for several hours. The $^{18}O_2$ and $H_2^{18}O$ (97% enriched ^{18}O, ISOTEC Co. Ltd.) was introduced in the other section, and the atmosphere was changed by connecting the cell to the other section at a constant temperature using six-way valves. The cell was quenched after a certain periods of isotope exchange. Since a little amount of O_2 or D_2O might be mixed even after changing the section, the ^{18}O concentration of gaseous phase was determined by using Quadra-pole mass spectrometer (RIGA 202P, ULVAC Co., Japan).

The gradient of ^{18}O concentration in the quenched sample was measured by collecting the intensities of the mass spectra at $M/e = 16$ and $M/e = 18$ by SIMS. The fraction of ^{18}O (X) in oxides were then calculated from the intensities (I/cps) of $^{16}O^-$ and $^{18}O^-$ ions.

$$X = I(^{18}O^-)/\{I(^{16}O^-) + I(^{18}O^-)\} \tag{1}$$

Oxygen isotope diffusivity ($D_O^*/m^2\ s^{-1}$) and surface exchange rate constant ($\alpha/m\ s^{-1}$) were determined by fitting depth profiles to the diffusion equation which was solved for semi-infinite media assuming surface reaction [14],

$$\frac{X - X_{bg}}{X_g - X_{bg}} = \mathrm{erfc}\frac{z}{2\sqrt{(D_O^* t)}} - \exp(bz + b^2 D_O^* t)\mathrm{erfc} \times \left\{\frac{z}{2\sqrt{(D_O^* t)}} + b\sqrt{(D_O^* t)}\right\} \tag{2}$$

$$b(m^{-1}) = \alpha / D_O^* \tag{3}$$

where X_g and X_{bg} are the isotope fractions in gaseous phase, and in background (=0.002), respectively, t (s) is the annealing time, and z (m) is the depth. The definition of the function "erfc" is:

$$\mathrm{erfc}(x) = 1 - \frac{2}{\sqrt{\pi}}\int_0^x \exp(-\eta^2)d\eta \tag{4}$$

Two types of analyses, i.e., line profiling and depth profiling were adopted to measure the ^{18}O fraction changes in the samples. Line profiles with the range of 10–250 μm were taken by scanning on the cross

section of the sample with relatively low energy primary beam ($I(Cs^+) = 1$ nA). The oxygen isotope diffusivity (D_O^*) can be determined with a good accuracy from the slopes of the line profiles. However, the absolute value of ^{18}O fraction (X) in the vicinity of surface is sometimes scattered, and it results low accuracy of the surface exchange rate constants. This scattering is caused by the adsorption of $^{16}O_2$ molecules on the measuring surface during the SIMS measurement. Hence, the depth profiles were also taken in shallow region (1–2 μm) by etching the sample surface with a high energy beam ($I(Cs^+) = 20$ nA) to measure the ^{18}O fraction at the surface with better accuracy.

3. Result and Discussion

3.1. *Hydrogen Solubility in* $\{(CeO_2)_x\ (ZrO_2)_{1-x}\}_{0.8}\ (YO_{1.5})_{0.2}$ *Polycrystals*

Figure 1 shows the secondary ion intensity ratio of deuterium ($^2D^-$) and oxygen ($^{16}O^-$) of $\{(CeO_2)_x(ZrO_2)_{1-x}\}(YO_{1.5})_{0.2}$ polycrystalline. Although we adopted two different temperatures for annealing, the obtained intensity ratio does not show any significant dependence on the annealing temperature. The logarithm of intensity ratio ($(I(^2D^-)/I(^{16}O^-))$) monotonically increased with cerium content (x), and has a maximum around $x = 0.8$.

In our previous papers, we reported that the deuterium intensity ratio in SIMS analyses has a linear relationship with the hydrogen content in the oxides [10, 15]. The apparent hydrogen concentration per volume (C_H/cm^{-3}) can be calculated from the intensity ratio with the following equation derived from our previous data of rare earth doped ceria [10].

$$\log(I(^2D^-)/I(^{16}O^-)) = \log(C_H/C_O) - 1.08 \quad (5)$$

The molar hydrogen concentration per 1 mole oxide ($C_{m,H}$) can be defined as $C_{m,H} = C_H V_m/N_m$, where V_m is the molar volume of oxide (cm^3/mol), N_m is the Abogadro's number (mol^{-1}). The calculated molar hydrogen concentration is plotted as a function of cerium content (x) in Fig. 2. The compositional dependence of hydrogen concentration can be described from the viewpoint of chemical potentials of constituent oxides in the solid solutions. Yokokawa et al. made thermodynamic calculation of C_H by taking into account the following equations assuming the first order of approximation [16].

$$YO_{1.5}\ (\text{in fluorite}) + 1/2H_2O = \ YOOH\ (\text{in fluorite}) \quad (6)$$

$$\mu(YO_{1.5}) + 0.5\{\mu^\circ(H_2O) + RT\ln p(H_2O)\} = \mu^\phi(YOOH) + RT\ln C(YOOH) \quad (7)$$

where the chemical potential of yttrium oxide ($\mu(YO_{1.5})$/J mol^{-1}) was evaluated from optimization of regular solution parameters to reproduce the observed phase separation, and the Henry constant for

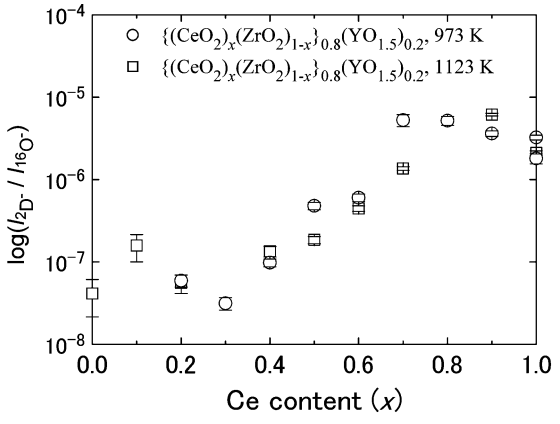

Fig. 1. Relative intensity of deuterium ion ($^2D^-$) against oxygen ion ($^{16}O^-$) detected by SIMS for $\{(CeO_2)_x(ZrO_2)_{1-x}\}_{0.8}(YO_{1.5})_{0.2}$ polycrystals annealed in 2% D_2O + 2% O_2 + 96% N_2 for 60 h.

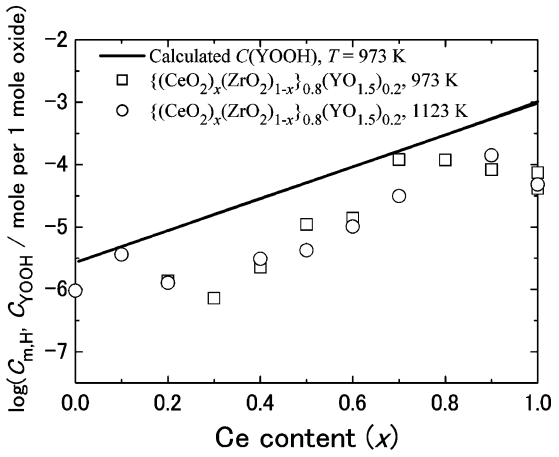

Fig. 2. Molar hydrogen solubility in $\{(CeO_2)_x(ZrO_2)_{1-x}\}_{0.8}$ $(YO_{1.5})_{0.2}$ polycrystals derived from deuterium intensity (symbols) and concentration of YOOH in oxides evaluated from thermodynamic analyses [16].

YOOH (μ^{ϕ}(YOOH)) was estimated from the data of similar hydroxides.

The calculated concentration of C(YOOH) at $T = 973$ K is shown as a solid line in Fig. 2, which has a similar dependence to that of $C_{\mathrm{m,H}}$. Although the possibility of the effect of grain boundary on the hydrogen solubility can not be denied, the good agreement between experimental $C_{\mathrm{m,\cdot H}}$ and calculated C(YOOH) indicates that the hydrogen dissolution mechanism is greatly affected by the thermodynamic characteristics of the bulk components. On the other hand, little dependence on annealing temperature on the experimental hydrogen solubility indicates that the diffusion of hydrogen might be very fast and the observed deuterium intensity ratio might be affected by the deuterium diffusion during the quenching procedures.

3.2. *Oxygen Isotope Diffusivity and Surface Exchange Rate for* $\{(CeO_2)_x(ZrO_2)_{1-x}\}_{0.8}(YO_{1.5})_{0.2}$

The data of oxygen isotope diffusivity (D_{O}^{*}) and surface exchange rate constant (α) of $\{(CeO_2)_x(ZrO_2)_{1-x}\}_{0.9}(Y_2O_3)_{0.1}$ at $T = 973$ K in dry $p(O_2) = 21$ kPa was reported by Naito et al. [8] and they are shown in Fig. 3 as circles. The data of surface exchange rate reported by Naito et al., have two maxima around $x = 0.2$ and 0.6. The exact reason of these two maxima was not clear. Hence, we reinvestigated the diffusivity and surface exchange rate constants from the data at $T = 973$ K at $p(O_2) = 21$ kPa, and plotted the results in Fig. 3 as the triangles. The reinvestigated data of surface exchange rate show a large maximum at around $x = 0.2$–0.3, and lower values were obtained for $x > 0.6$.

The presently obtained data of oxygen isotope diffusivity and surface exchange rate constant of $\{(CeO_2)_x(ZrO_2)_{1-x}\}_{0.8}(YO_{1.5})_{0.2}$ at $T = 973$ K, in a humid atmosphere ($p(H_2O) = 2$ kPa, $p(O_2) = 7$ kPa) were shown in Fig. 3 as squares. The surface reaction data seems to slightly increase with cerium content (x), however the compositional dependence was very small.

Since α value is determined by $b = \alpha/D_{\mathrm{O}}^{*}$ in Eqs. (2) and (3) and it is influenced by the absolute value of D_{O}^{*}, the parameter b was plotted as a function of cerium content (x) in Fig. 4 to exhibit the difference of the surface reaction rates more clearly. It is obvious that the b values in a humid atmosphere (open squares) are higher than those in air. However, the difference between the presently observed data and Naito's original data was relatively small.

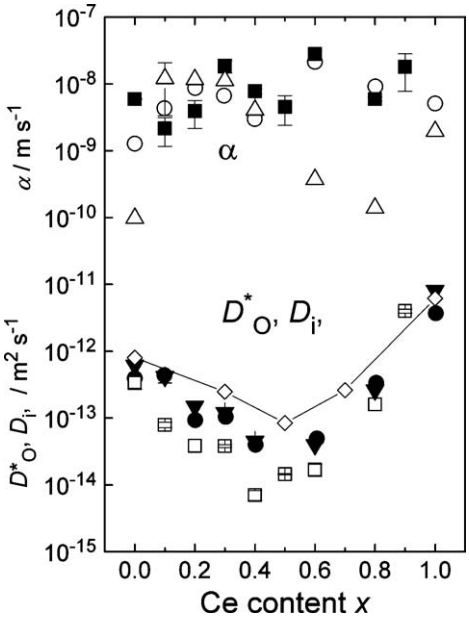

Fig. 3. Oxygen exchange rate constant (α) and oxygen isotope diffusivity (D_{O}^{*}) of $\{(CeO_2)_x(ZrO_2)_{1-x}\}_{0.8}(YO_{1.5})_{0.2}$ at $T = 973$ K: ○, ● $p(O_2) = 21$ kPa from Naito et al. [8], △, ▼ reinvestigated data, $p(O_2) = 21$ kPa, and ■, □ $p(H_2O) = 2$ kPa, $p(O_2) = 7$ kPa. ◇ D_i derived from total conductivity in air, $T = 973$ K.

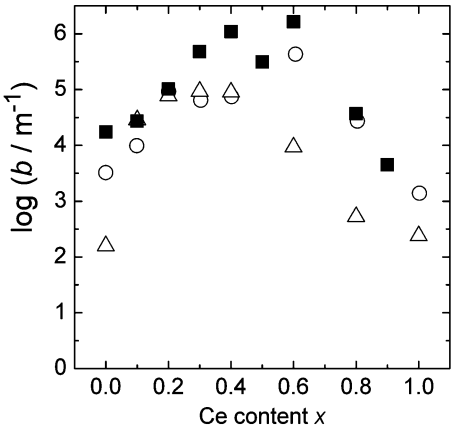

Fig. 4. Parameter b ($= \alpha/D_{\mathrm{O}}^{*}$) as a function of cerium content (x): ○, $p(O_2) = 21$ kPa from Naito et al. [8], △, reinvestigated data, $p(O_2) = 21$ kPa, and ■, $p(H_2O) = 2$ kPa, $p(O_2) = 7$ kPa.

The compositional dependence of surface exchange rate having maxima is similar to that observed in the electronic conductivity ($\sigma_{\mathrm{electron}}$) of $\{(CeO_2)_x(ZrO_2)_{1-x}\}_{0.8}(YO_{1.5})_{0.2}$ determined by a

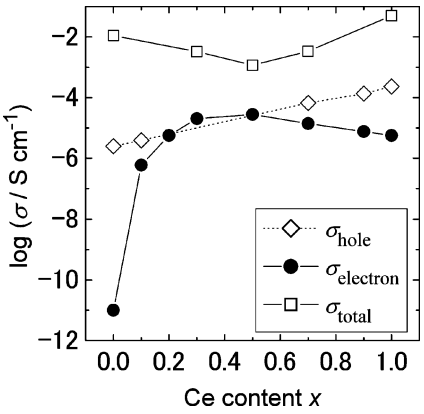

Fig. 5. Conductivity of $\{(CeO_2)_x(ZrO_2)_{1-x}\}_{0.8}(YO_{1.5})_{0.2}$ at $T = 1073$ K in air as a function of cerium content (x). Some of $\sigma_{electron}$ data are estimated by the extrapolation of the data in reducing atmosphere.

blocking method by Xiong et al. as shown in Fig. 5 [16, 17]. The oxygen exchange reaction on oxide surface can be expressed by the following equations:

$$1/2\,{}^{18}O_2(g) \rightleftarrows {}^{18}O_{ad} \tag{8a}$$

$${}^{16}O_O^{\times}\ (\text{in oxide}) \rightleftarrows {}^{16}O''_{ad} + V_O^{\bullet\bullet} \tag{8b}$$

$${}^{18}O_{ad} \rightleftarrows {}^{18}O''_{ad} + 2h^{\bullet}\ (\text{in oxide}) \tag{8c}$$

$$\text{or } {}^{18}O_{ad} + 2e'(\text{in oxide}) \rightleftarrows {}^{18}O''_{ad} \tag{8c'}$$

$${}^{16}O''_{ad} + 2h^{\bullet}\ (\text{in oxide}) \rightleftarrows {}^{16}O_{ad} \tag{8d}$$

$$\text{or } {}^{16}O''_{ad} \rightleftarrows {}^{16}O_{ad} + 2e'\ (\text{in oxide}) \tag{8d'}$$

$${}^{18}O''_{ad} + V_O^{\bullet\bullet} \rightleftarrows {}^{18}O_O^{\times}(\text{in oxide}) \tag{8e}$$

If the electron concentration in oxides is higher than hole concentration, the processes (8c′) and (8d′) replace (8c) and (8d). In any case, the reaction rates of these processes should greatly depend on the hole or electronic conductivity. The similarity of compositional dependence of oxygen isotope exchange rate (α) and electronic conductivity suggests that the processes (8c) or (8d) should be the rate determining step of the oxygen exchange reaction on the $\{(CeO_2)_x(ZrO_2)_{1-x}\}_{0.8}(YO_{1.5})_{0.2}$ surface.

Concerning the effect of water vapor addition, it should be noted that the oxygen surface exchange rate constant (α) of YSZ or GDC drastically increased by water vapor addition at $T = 973$ K [12, 13]. However in the present data, the difference of surface exchange rate constant (α) between a humid and dry air is not large in the region of $x = 0.1$–0.6. It indicates that the effect of increasing electronic conductivity is more significant in that region. In contrast, the surface exchange rate constant considerably increased in humid atmospheres for cerium-rich composition ($x > 0.6$). It may indicate that a considerable amount of water may dissolve in the samples and it may affect on the oxygen exchange mechanisms on the surface. However, the difference between the present data and Naito's original data is not large, which suggests that there might be some difficulty in control water vapor pressure.

The compositional dependence of oxygen isotope diffusivity (D_O^*) is similar among all series of data as shown in Fig. 3. These diffusivities are compared with the oxygen self diffusivity (D_i/m^2 s^{-1}) calculated from oxide ion conductivity by using the modified Nernst-Einstein equation:

$$D_i = \frac{V_m RT\sigma_i}{yZ^2F^2} \tag{9}$$

$$D_O^* = fD_i \tag{10}$$

where V_m is the molar volume (m^3 mol^{-1}), R is the gas constant (J mol^{-1} K^{-1}), T is the temperature (K), σ_i is the ionic conductivity (S m^{-1}), y is the oxygen content (=1.9 for 1 mole of $\{(CeO_2)_x(ZrO_2)_{1-x}\}_{0.8}(YO_{1.5})_{0.2}$), Z is the valence number of charge carrier (=2 for oxide ion), and F is the Faraday constant (C mol^{-1}), and f is the correlation factor. The molar volume of $\{(CeO_2)_x(ZrO_2)_{1-x}\}_{0.8}(YO_{1.5})_{0.2}$ was calculated from the lattice constants reported by us [18]. The calculated D_i data are plotted in Fig. 3, and D_i and D_O^* data are in good agreement if the correlation factor was assumed to be 0.66.

4. Conclusion

The hydrogen solubility, oxygen isotope diffusivity and surface exchange rate was determined by SIMS for ceria-zirconia-yttria solid solutions $\{(CeO_2)_x(ZrO_2)_{1-x}\}_{0.8}(YO_{1.5})_{0.2}$ at 973–1173 K. The following facts should be emphasized:

(1) The results of deuterium ion intensity measured by SIMS exhibited that a considerable amount of water can be dissolved in a ceria rich region. The deuterium intensity ratio $\log\{I(^2D^-)/I(^{16}O^-)\}$ increased linearly with the cerium content (x) in the range of $x = 0.2$–0.8.

(2) The reinvestigated data of oxygen exchange rate on $\{(CeO_2)_x(ZrO_2)_{1-x}\}_{0.8}(YO_{1.5})_{0.2}$ in air at $T = 973$ K has a maximum at $x = 0.2$–0.3, which can be correlated with the compositional dependence of electronic conductivity.
(3) The oxygen isotope diffusivity in $\{(CeO_2)_x(ZrO_2)_{1-x}\}_{0.8}(YO_{1.5})_{0.2}$ has a minimum at $x = 0.5$, which is in good agreement with the compositional dependence of total conductivity.
(4) The large difference and scattering were observed among the surface exchange rate constants in dry air and a humid atmosphere, which may indicate the effect of water dissolution in $\{(CeO_2)_x(ZrO_2)_{1-x}\}_{0.8}(YO_{1.5})_{0.2}$ polycrystals.

Acknowledgment

The part of this work is supported by NEDO International Joint Research Grant, "Efficient and Flexible SOFC System".

References

1. M. Mogensen, T. Lindegaad, and U.R. Hansen, *J. Electrochem. Soc.*, **141**, 2122 (1994).
2. T. Horita, N. Sakai, H. Yokokawa, M. Dokiya, T. Kawada, and K. Sasaki, *J. Electroceramics*, **1**(2), 155 (1997).
3. K. Eguchi, T. Setoguchi, T. Inoue, and H. Arai, *Solid State Ionics*, **52**, 165 (1992).
4. C. Bozo, N. Guilhaume, E. Garbowski, and M. Primet, *Catalysis Today*, **59**, 33 (2000).
5. B. Calès and J.F. Baumard, *J. Electrochem. Soc.*, **131**(10), 2407 (1984).
6. H. Arashi, H. Naito, and M. Nakata, *Solid State Ionics*, **76**, 315 (1995).
7. P.V. Ananthapadmanabhan, N. Venkatramani, V.K. Rohatgi, A.C. Momin, and K.S. Venkateswarlu, *J. Eur. Ceram. Soc.*, **6**, 111 (1990).
8. H. Naito, N. Sakai, T. Otake, H. Yugami, and H. Yokokawa, *Solid State Ionics*, **135**, 669 (2000).
9. Y. Xiong, K. Yamaji, N. Sakai, H. Negishi, T. Horita, and H. Yokokawa, *J. Electrochem. Soc.*, **148**(12), E489 (2001).
10. N. Sakai, K. Yamaji, T. Horita, H. Yokokawa, Y. Hirata, S. Sameshima, Y. Nigara, and J. Mizusaki, *Solid State Ionics*, **125**, 325 (1999).
11. N. Sakai, K. Yamaji, H. Negishi, T. Horita, H. Yokokawa, Y.P. Xiong, and M.B. Phillipps, *Electrochemistry*, **68**(6), 499 (2000).
12. N. Sakai, K. Yamaji, T. Horita, Y.P. Xiong, H. Kishimoto, H. Yokokawa, *J. Electrochem. Soc.*, **150**(6), A689 (2003).
13. N. Sakai, K. Yamaji, T. Horita, H. Kishimoto, Y.P. Xiong, and H. Yokokawa, *Phys. Chem. Chem. Phys.*, **5**, 2253 (2003).
14. J. Crank, *The Mathematics of Diffusion*, 2nd ed., (Oxford Science Publications, Oxford University Press, Oxford, 1975), p. 22.
15. N. Sakai, K. Yamaji, T. Horita, and H. Kishimoto, Y.P. Xiong, H. Yokokawa, *Solid State Ionics*, in press.
16. K. Sasaki, K. Watanabe, and Y. Teraoka, *J. Electrochem. Soc.*, **151**(7), A965 (2004).
17. Y.P. Xiong, K. Yamaji, T. Horita, N. Sakai, and H. Yokokawa, *unpublished data*.
18. N. Sakai, T. Hashimoto, T. Katsube, K. Yamaji, H. Negishi, T. Horita, H. Yokokawa, Y.P. Xiong, M. Nakagawa, and Y. Takahashi, *Solid State Ionics*, **143**, 151 (2001).